

Fast tomography using quasi-monochromatic undulator radiation

Kentaro Uesugi,* Toshihiro Sera and Naoto Yagi

Received 27 December 2005

Accepted 19 June 2006

SPring-8/JASRI, 1-1-1 Kouto, Sayo, Hyogo 679-5198, Japan. E-mail: ueken@spring8.or.jp

A beamline with a helical undulator has been used without a monochromator for fast high-resolution tomographic imaging with an X-ray energy of 12.4–16.5 keV and an energy bandwidth of 2–3%. The X-ray beam was expanded with two mirrors to 12 mm × 4 mm. The X-ray field was made uniform by a diffuser. The detector pixel size was 9.9 μm × 9.9 μm. At the highest speed, a 180° scan was completed in 6 s with 454 projections. Beam-hardening effects were not significant. This technique may be useful in studying time-dependent structural changes of soft materials such as polymers and biological samples.

© 2006 International Union of Crystallography
Printed in Great Britain – all rights reserved

Keywords: tomography; helical undulator; fast scan; soft materials.

1. Introduction

X-ray microtomography is a non-destructive technique which enables investigation of the three-dimensional structure of an object. Experimentally, a series of digital radiograms at different angular positions of the sample is recorded, and reconstruction of the three-dimensional structure is obtained by using a mathematical procedure such as filtered back-projection. It has been widely used at synchrotron radiation facilities in the fields of, for instance, polymer science, metallurgy, hydrology, earth and planetary science, biology and medicine (Spanne & Rivers, 1987; Bonse & Busch, 1996). The advantages of synchrotron monochromatic computed tomography (CT) are (i) owing to the small source size, high spatial resolution can be achieved, (ii) beam-hardening effects, which are serious with white X-rays, are minimal. When the specimen is a soft material that may deform with time, or when time-resolved imaging is required, it is necessary to scan the sample as quickly as possible. In such cases the second advantage is often sacrificed by using a white X-ray beam (Lame *et al.*, 2003; Di Michiel *et al.*, 2005). However, beam-hardening effects considerably reduce the merit of the technique. Especially with a soft matter, the contrast between materials can be small, necessitating high-density resolution. Also, with a white beam it is difficult to make use of an absorption edge of an element to visualize its distribution.

The beam-hardening problem may be circumvented by using a quasi-monochromatic X-ray beam from an undulator such as BL40XU at SPring-8. The X-ray source of this beamline is a helical undulator, which produces only weak harmonics on its radiation axis (Hara *et al.*, 2001). Thus, by using the central part of the radiation a quasi-monochromatic X-ray beam with an energy bandwidth of 2–3% (full width at a half-maximum) in the energy range 8.1–16.5 keV is obtained (Inoue *et al.*, 2001). This radiation is used without monochromatization after effectively eliminating the harmonics by

total reflection on two mirrors which are also used for focusing.

In the present study we used this beamline for high-resolution high-speed CT. Since most tomographic experiments require a large field of view rather than a focused beam, we expanded the beam using another two over-bent mirrors. The X-ray bandwidth was found to be narrow enough to make the beam-hardening effects insignificant. The shortest scan time was 6 s, which was limited by the speed of the rotation stage. This technique is considered to be useful for time-resolved CT of soft materials such as polymers and biological specimens. When the contrast between materials is too low, phase-imaging techniques may be employed to enhance the contrast (Cloetens *et al.*, 1999; Sera *et al.*, 2005).

2. Methods

Radiation from the helical undulator at BL40XU in SPring-8 was used without monochromatization. The storage ring was run in top-up mode with a fixed current of 99 mA. The crossed slits in the front-end were closed to restrict the radiation to less than 5 μrad vertically and 15 μrad horizontally. The two mirrors that were designed for focusing were used as flat mirrors to remove harmonics. The first mirror, coated with Ni, reflected X-rays horizontally at a glancing angle of 3 mrad, and the second mirror, coated with Rh, reflected X-rays vertically at a glancing angle of 4 mrad. The total flux of this beamline under these conditions was 6×10^{14} photons s⁻¹ at 15 keV (Inoue *et al.*, 2001).

The set-up in the experimental hutch is shown in Fig. 1. Two Pt-coated mirrors (20 cm long) were placed in tandem. The first one reflected the X-rays in the horizontal direction while the second one reflected them in the vertical (downward) direction. The mirrors were bent with a four-point bending mechanism (Franks, 1955). To make the X-ray field as even as possible, a diffuser was introduced upstream of the first mirror.

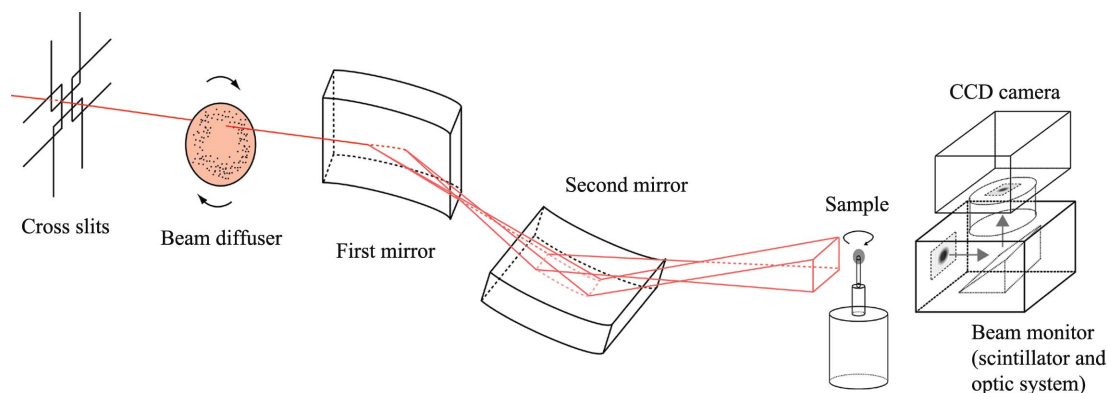


Figure 1

Schematic drawing of the experimental set-up. All components were in the experimental hutch. The cross slits defined the beam and reduced scatter from upstream optical and mechanical elements, such as shutters and absorbers. The diffuser can be placed either upstream of the first mirror or between the second mirror and the sample, with similar effects. The small undulator beam is expanded by the two over-bent mirrors both horizontally and vertically.

This diffuser (Takeuchi *et al.*, 2002) is made of a 5 mm-thick layer of a graphite powder and rotates at a speed of 1000–3000 r.p.m.

For alignment of the X-ray beam, a CMOS flat-panel detector (C7942, Hamamatsu Photonics, Hamamatsu, Japan; Yagi, Yamamoto *et al.*, 2004) was used. For recording images, a CCD-based high-resolution detector ('beam monitor 2'; AA20, Hamamatsu Photonics; Uesugi *et al.*, 2001) was used with an interline CCD camera (C4880-80-24A, Hamamatsu Photonics) which has 656×494 pixels (each pixel is $9.9 \mu\text{m} \times 9.9 \mu\text{m}$). The lens in the X-ray detector had a focal length of 50 mm and the same lens was used with the camera, so that the pixel size was $9.9 \mu\text{m} \times 9.9 \mu\text{m}$ on the phosphor. The phosphor in the X-ray detector was 20 μm -thick P43 ($\text{Gd}_2\text{O}_2\text{S:Tb}$) which absorbed 40–60% of X-rays in the energy range 12.4–16.5 keV. The decay time of the fluorescence of the phosphor is 1–2 ms (Yagi, Inoue & Oka, 2004). The frame rate of the camera depends on the size of the field. It is 28 frames s^{-1} (36 ms frame⁻¹) with the full frame and 77 frames s^{-1} (13 ms frame⁻¹) with 656×120 pixels. Thus, the higher frame rate is made possible by reducing the field of view, not by reducing the spatial resolution (*i.e.* by binning). Since this camera is an interline type, it does not require an X-ray shutter for readout. A new image can be acquired while the image in the previous frame is being transferred to a frame grabber (IC-PCI, DALSA Coreco, Saint-Laurent, Canada). The computer had a Pentium 4 CPU (2.8 GHz) and 2 GB memory with a standard 32-bit PCI bus.

In the CT experiment, the sample was placed on a rotation stage (SGSP-60YAW, Sigma-Koki, Tokyo, Japan) with the axis set vertically. The rotation axis was aligned parallel to the column of the pixels in the CCD. The stage was rotated continuously during the CT scan. The X-ray detector recorded projection images continuously. The detector was at about 10 cm from the sample. The rotation angle and the frame timing were correlated after the experiment by using TTL pulses from the stage controller (MARK-204, Sigma-Koki) and the CCD camera, which were recorded at 1 kHz sampling with a data-acquisition system based on *LabView* (National Instruments, Austin, TX, USA).

The acquired images were normalized with a flat-field image without a specimen after being corrected for the dark current. Reconstruction of tomographic images was carried out with a conventional algorithm using a convolution back-projection. The software is available from <http://www-bl20.spring8.or.jp/>.

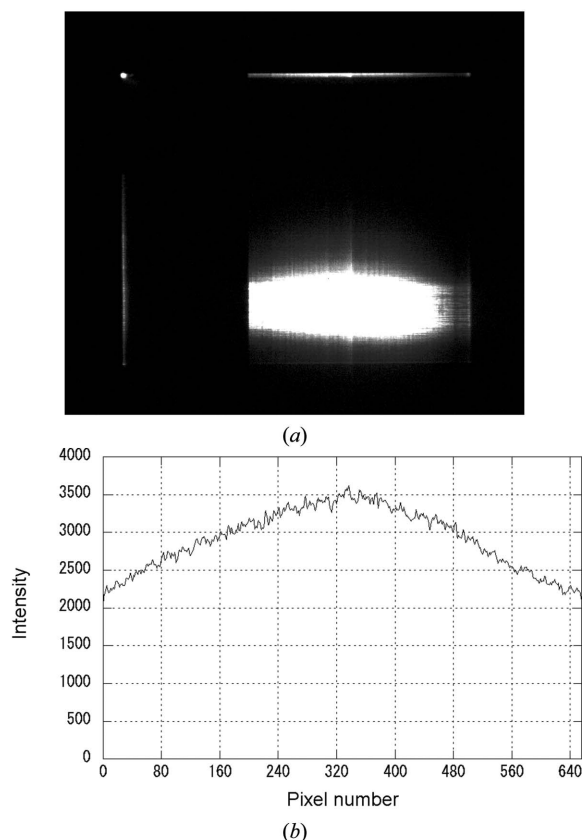
3. Results

3.1. X-ray techniques

By over-bending the two mirrors in the experimental hutch it was possible to expand the X-ray beam, which was originally 0.4 mm horizontally by 0.15 mm vertically at the mirrors, to a size of 12 mm horizontally by 4 mm vertically (Fig. 2*a*). The X-rays were reflected by the two mirrors with a glancing angle of 3.5 mrad (the X-ray energy was 12.4 keV). The distance from the center of the two mirrors to the detector was about 3.3 m. This beam size is not the largest achievable. It is possible to expand the beam to twice this size, both horizontally and vertically, but this was unnecessary for the purpose of the current study because the detector area would be smaller than the beam size.

Since the projection images are normalized by a flat-field image, a uniform intensity distribution is not mandatory for CT. However, to fully make use of the dynamic range of the CCD-based X-ray detector (which is especially narrow, about 1000, with the fast camera used in this study), it is desirable to make the X-ray field as uniform as possible. In the present experiment the beam expanded by the mirrors was quite uneven with sharp intensity minima and maxima due to slope errors in the surface profiles of the mirrors. To make it smoother, a diffuser was introduced upstream of the mirrors. With the use of the diffuser the flatness of the expanded beam was acceptable (Fig. 2*b*).

The X-ray flux in the central (15 μrad horizontally, 5 μrad vertically) area of the radiation at this beamline is $1 \times 10^{15} \text{ photons s}^{-1}$ with the fundamental radiation at 12.4 keV. The bandwidth is 2% at 12.4 keV (Inoue *et al.*, 2001). When the beam is expanded to 12 mm \times 4 mm, the flux is about $1.5 \times 10^{13} \text{ photons s}^{-1} \text{ mm}^{-2}$, giving $1.5 \times 10^9 \text{ photons s}^{-1}$ for each

**Figure 2**

X-ray beam recorded with a CMOS flat-panel detector (C7942, Hamamatsu Photonics) at the sample position. (a) Overview of the expanded beam. The spot at the top left is part of the direct beam. The horizontal beam at the top is the beam reflected by the horizontal mirror but not by the vertical mirror, while the vertical beam on the left is one not reflected by the horizontal mirror but reflected by the vertical mirror. The large rectangular bright area is the beam reflected by both mirrors. The peak X-ray energy was 12.4 keV. The field of view is 52 mm \times 45 mm. (b) Horizontal intensity profile of part of the enlarged beam.

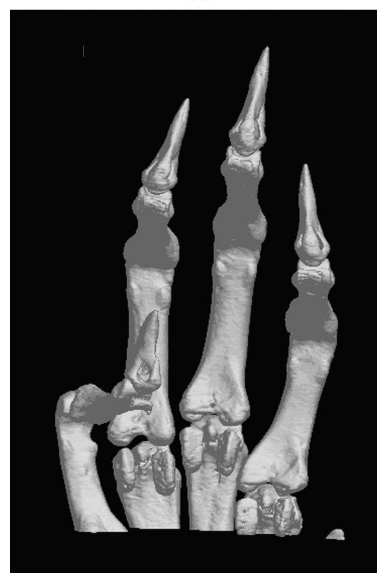
pixel (10 μm \times 10 μm). The reflectivity of the mirrors, and absorption by the diffuser and air, may reduce this flux by about tenfold (exact reflectivity and absorption depend on the X-ray energy). Since the X-ray detector saturates with about 3000 X-ray photons at 12.4 keV, even at the fastest frame rate in this experiment (77 frames s^{-1} , see below), the flux was still about 10^2 times too high. Thus, the intensity was adjusted by closing the two slits in the front-end of the beamline or by using Al absorbers so that the direct beam almost saturated the detector with the given exposure time.

3.2. Computed tomography examples

Test experiments were made on several soft material samples. One was the middle finger of the hind leg of a mouse (Fig. 3a). It was recorded at 16.5 keV to ensure penetration of X-rays through a bone. The flux was reduced to about 5% with Al absorbers. A series of 1365 projections was recorded over 180° with a full frame (656 \times 494 pixels). The exposure time for each projection was 35 ms and the total exposure time was 48 s. The total dose on the sample was about 150 Gy. Since the



(a)



(b)

Figure 3

Reconstructed cross section and three-dimensional structure of mouse digits. The sample was from an animal that was sacrificed for a different experiment, kept frozen, and warmed just before the experiment. With a peak X-ray energy of 16.5 keV, 1365 projections were continuously recorded over 180°. The total exposure time was 48 s. (a) Cross section of a middle digit of a hind leg. One side of the image is 2.2 mm. (b) Three-dimensional reconstruction of a paw of a foreleg. The image size is 3.9 mm \times 5.6 mm.

images were continuously recorded, the total exposure time was the same as the time required for the data collection. Skin, bone and hairs are clearly resolved.

An entire paw of a mouse foreleg was also imaged. Fig. 3(b) is a three-dimensional reconstruction by surface rendering. The density cut-off level is adjusted to show only the bones. Detailed structure of bones and joints can be observed clearly.

In order to assess the effect of beam hardening, a resin rod of uniform density was imaged at 15 keV (Fig. 4). An effect of beam hardening, which lowers the apparent density in the center of the rod and enhances that in the periphery, was not evident in the image. However, quantitative measurement of the linear attenuation coefficient (LAC) showed that the LAC value in the center was $1.2957 \pm 0.0008 \text{ cm}^{-1}$ while that in the periphery was $1.3059 \pm 0.0008 \text{ cm}^{-1}$ (mean and the standard error of the mean, $N = 54000$ pixels in each region). The difference (0.8%) is statistically significant but smaller than the density resolution of the monochromatic CT system, which has been estimated to be about 1% (Torikoshi *et al.*, 2003). Thus, the beam-hardening effect, which is expected from the

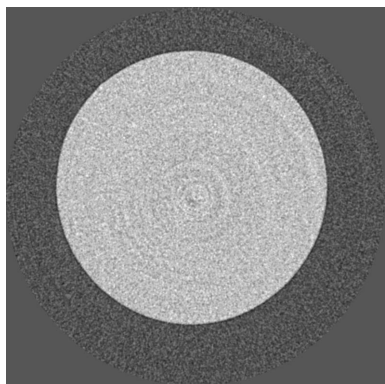
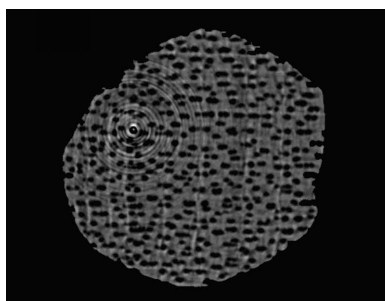
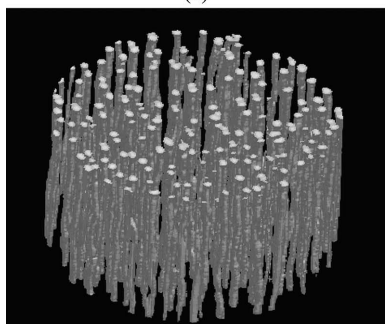


Figure 4
Reconstructed cross section of a resin rod, measured with a peak X-ray energy of 15.0 keV and 312 projections (each exposure was 32 ms). The image size is 3.1 mm × 3.1 mm. The image is purposely contrasted to show details in the density variation.



(a)



(b)

Figure 5
Reconstructed cross section and three-dimensional structure of a wood stick whose diameter was about 3.1 mm. (a) Cross section. (b) Three-dimensional reconstruction by volume rendering. The area with low density (air) is visualized.

use of a non-monochromatic beam (3% bandwidth at 15 keV), does not affect the density (LAC) resolution appreciably.

To test faster recording, a dried wood stick was used as a test specimen (Fig. 5a). It was imaged at 12.4 keV. By reducing the number of pixels in the camera to 656 × 120, the exposure time for each projection was 13 ms and the total exposure time was 6 s. The flux was reduced to about 1% with Al absorbers. This attenuation was higher than that at 16.5 keV because the detector saturated with the shorter exposure time at 12.4 keV. This is due to the higher flux and higher detector efficiency at the lower energy. A series of 454 projections was recorded over 180°. The total dose was about 44 Gy. The ring artefacts can be suppressed by a numerical filter (Raven, 1998) but a

raw image is shown here. Many small holes and parts of annual rings are seen in the reconstructed cross section (Steppe *et al.*, 2004). A three-dimensional reconstruction to visualize the low-density region (Fig. 5b) shows that these holes are mostly continuous throughout the height of the view (1.2 mm).

4. Discussion

Use of the quasi-monochromatic radiation from an undulator in the present study contrasts that of white radiation from a wiggler in previous reports on fast CT (Lame *et al.*, 2003; Di Michiel *et al.*, 2005). Generally, there are three major differences between undulators and wigglers: (i) beam size, (ii) energy range, (iii) energy spread. Since wigglers have a larger beam divergence, it is unnecessary to expand the beam for CT. On the other hand, as the flux density of an undulator beam is much higher, an undulator has the potential to be used at higher spatial and time resolution. As for the beam energy range, at third-generation synchrotron radiation facilities the radiation from wigglers usually has higher energy than the fundamental radiation of undulators. Thus, wigglers are more useful for heavy elements such as metals than undulators, which are more useful for soft materials with lower density. Wide energy spread of white radiation from a wiggler poses the problem of low density contrast and beam hardening. Although a reasonable contrast (signal-to-noise ratio) is obtained in the case of metal alloys with a large density difference (Di Michiel *et al.*, 2005), it is difficult to distinguish materials with similar densities. Also, images obtained with white radiation are not free from beam-hardening effects. The narrow bandwidth of undulator radiation ensures high contrast (*i.e.* high density resolution). It is demonstrated here that the beam-hardening effect is indeed very small (Fig. 4). Since a bandwidth similar to that used in the present experiment (about 2%) can be obtained with a multilayer monochromator (Chu *et al.*, 2002), it may be used with wigglers and bending magnets to avoid beam-hardening effects.

Although the scan time achieved here, 6 s, is much shorter than in most CT experiments using synchrotron radiation, it is not fast enough when the specimen is not static. In a medical CT system, a scan time shorter than 1 s has been achieved to avoid movements due to heartbeats. In the present experiment the X-ray beam was attenuated 100–1000-fold to avoid saturation of the detector. Thus, if the sample can be rotated faster, the total data-acquisition time can be further reduced. Use of a 3-CCD camera (Yagi, Inoue & Oka, 2004) makes it possible to record 390 frames (640 × 480 pixels) per second. Thus, a scan time shorter than 1 s is realistic. In order to make the best use of the high flux, an ultrafast CMOS camera with a large amount of memory has to be used. Although a frame rate higher than 10000 s⁻¹ may be achieved, stable rotation of a sample at high speed would be the most serious difficulty in such an experiment. Also, radiation damage in soft material samples may be serious. Such samples often have low heat conductance and thus the temperature rise is more pronounced at a higher dose rate.

It is also possible to use the high flux to increase the spatial resolution. By using an imaging detector with higher resolution (Cloetens *et al.*, 2002; Uesugi *et al.*, 2001; Wang *et al.*, 2001), a fast scan can be performed with submicrometer pixel size. Fresnel-zone-plate optics has already been tested at this beamline (Suzuki *et al.*, 2004) and can be used for submicrometer-resolution CT. In these cases the most limiting factor will be the radiation damages on the sample, the phosphor in the X-ray detector and/or X-ray optical devices. Also, high spatial resolution requires stable and precise rotation of the sample.

It should be pointed out that, if shorter scan time or higher spatial resolution is not required, this technique can also be used at an undulator beamline with a monochromator. A monochromatic undulator beamline at a third-generation synchrotron radiation facility usually provides a total flux of 10^{12} – 10^{13} photons s^{-1} . When these photons are spread over, say, 1000×1000 pixels, each pixel receives 10^6 – 10^7 photons s^{-1} . If the framing rate during a CT scan is $30 s^{-1}$, there are 3×10^4 – 3×10^5 photons in each pixel. This is enough to obtain an image with a reasonable signal-to-noise ratio, even considering a loss associated with expansion of the beam (such as low reflectivity of mirrors and absorption by a diffuser in the present experiment).

Although it is not essential, the mirrors should be improved to obtain a smoother field of view. A better fabrication technique (Yamauchi *et al.*, 2003) will improve the uniformity of the intensity distribution in the expanded X-ray beam. This will make a diffuser unnecessary and help increase the flux at the sample.

One practical limit in the present experiment was the repetition rate of the measurements. The CCD camera (C4880-80) transfers data at a rate of $9.4 \text{ Mpixels s}^{-1}$. This is kept constant when the frame rate is increased by reducing the size of view. Thus, the total amount of data for Fig. 3(b) was 850 Mbytes and that for Fig. 4 was 112 Mbytes, in proportion to the total data-acquisition time. Although these data could be stored in the computer memory during the experiment, transfer to a hard disk took longer than the scan itself. Thus, the repetition rate of the experiment was limited by the data transfer. Since the practical time resolution is defined by the time between successive CT scans, this is a serious drawback. As the 3-CCD camera mentioned above has a data rate of about $90 \text{ Mpixels s}^{-1}$, the demand on the computer memory and the data transfer to a disk is more severe. Use of a more sophisticated computer system (Di Michiel *et al.*, 2005) will help to solve this problem to some extent. Ideally the data should be sent to a hard disk during recording but this requires a specialized data-acquisition system. On top of this, in order to achieve high-throughput data processing it is desirable to construct a system that makes use of parallel computing methods for image reconstruction (Wang *et al.*, 2001).

The technique developed in the present work is suitable for studies on three-dimensional structures of soft materials, including biological samples, which are readily deformed during a long scan. It will be a particularly useful tool for studying morphological deformation of samples induced by heating (for example, phase separation in metals and polymers).

We thank Dr Yoshio Suzuki for use of the diffuser. The experiments were performed under approval of the SPring-8 Proposal Review Committee (2004B0053-NM-np).

References

- Bonse, U. & Busch, F. (1996). *Prog. Biophys. Mol. Biol.* **65**, 133–169.
- Chu, Y. S., Liu, C., Mancini, D. C., De Carlo, F., Macrander, A. T., Lai, B. & Shu, D. (2002). *Rev. Sci. Instrum.* **73**, 1485–1487.
- Cloetens, P., Ludwig, W., Baruchel, J., Van Dyck, D., Van Landuyt, J., Guigay, J. P. & Schlenker, M. (1999). *Appl. Phys. Lett.* **75**, 2912.
- Cloetens, P., Ludwig, W., Boller, E., Helfen, L., Alvo, L., Mache, R. & Schlenker, M. (2002). *Proc. SPIE*, **4503**, 82–91.
- Di Michiel, M., Merino, J. M., Fernandez-Carreiras, D., Buslaps, T., Honkimäki, V., Falus, P., Martins, T. & Svensson, O. (2005). *Rev. Sci. Instrum.* **76**, 043702.
- Franks, A. (1955). *Proc. Phys. Soc. London*, **B68**, 1054–1064.
- Hara, T., Tanaka, T., Seike, T., Bizen, T., Maréchal, X., Kohda, T., Inoue, K., Oka, T., Suzuki, T., Yagi, N. & Kitamura, H. (2001). *Nucl. Instrum. Methods*, **A467–468**, 165–168.
- Inoue, K., Oka, T., Suzuki, T., Yagi, N., Takeshita, K., Goto, S. & Ishikawa, T. (2001). *Nucl. Instrum. Methods*, **A467–468**, 674–677.
- Lame, O., Bellet, D., Di Michiel, M. & Bouvard, D. (2003). *Nucl. Instrum. Methods*, **B200**, 287–294.
- Raven, C. (1998). *Rev. Sci. Instrum.* **69**, 2978–2980.
- Sera, T., Uesugi, K. & Yagi, N. (2005). *Med. Phys.* **32**, 2787–2792.
- Spanne, P. & Rivers, M. L. (1987). *Nucl. Instrum. Methods*, **B24–25**, 1063–1067.
- Steppe, K., Cnudde, V., Girard, C., Leneur, R., Cnudde, J.-P. & Jacobs, P. (2004). *J. Struct. Biol.* **248**, 11–21.
- Suzuki, Y., Takeuchi, A., Takano, H., Uesugi, K., Oka, T. & Inoue, K. (2004). *Rev. Sci. Instrum.* **75**, 1155–1157.
- Takeuchi, A., Uesugi, K., Takano, H. & Suzuki, Y. (2002). *Rev. Sci. Instrum.* **73**, 4246–4249.
- Torikoshi, M., Tsunoo, T., Sasaki, M., Endo, M., Noda, Y., Ohno, Y., Kohno, T., Hyodo, K., Uesugi, K. & Yagi, N. (2003). *Phys. Med. Biol.* **48**, 673–685.
- Uesugi, K., Suzuki, Y., Yagi, N., Tsuchiyama, A. & Nakano, T. (2001). *Nucl. Instrum. Methods*, **A467–468**, 853–856.
- Wang, Y., Carlo, F. D., Mancini, D. C., McNulty, I., Tieman, B., Bresnahan, J., Foster, I., Insley, J., Lane, P., von Laszewski, G., Kesselman, C., Su, M. & Thiebaut, M. (2001). *Rev. Sci. Instrum.* **72**, 2062–2068.
- Yagi, N., Inoue, K. & Oka, T. (2004). *J. Synchrotron Rad.* **11**, 456–461.
- Yagi, N., Yamamoto, M., Uesugi, K. & Inoue, K. (2004). *J. Synchrotron Rad.* **11**, 347–352.
- Yamauchi, K., Yamamura, K., Mimura, H., Sano, Y., Saito, A., Endo, K., Souvorov, A., Yabashi, M., Tamasaku, K., Ishikawa, T. & Mori, Y. (2003). *Jpn. J. Appl. Phys.* **42**, 7129–7134.